Available online at www.sciencedirect.com
SCIENCE DIRECT®
Journal of Crystal Growth 260 (2004) 388–393
JOURNAL OF CRYSTAL GROWTH
www.elsevier.com/locate/jcrysgro

Structural and optical properties of quaternary AlInGaN epilayers grown by MOCVD with various TMGa flows

J.P. Liu[a,*], B.S. Zhang[a], M. Wu[a], D.B. Li[b], J.C. Zhang[a], R.Q. Jin[a], J.J. Zhu[a], J. Chen[a], J.F. Wang[a], Y.T. Wang[a], H. Yang[a]

[a] *State Key Laboratory on Integrated Optoelectronics, Institute of Semiconductors, Chinese Academy of Sciences, P.O. Box 912, Beijing 100083, China*

[b] *Key Laboratory of Semiconductor Materials, Institute of Semiconductors, Chinese Academy of Sciences, P.O. Box 912, Beijing 100083, China*

Received 29 July 2003; accepted 5 September 2003
Communicated by M. Schieber

Abstract

AlInGaN quaternary epilayers have been grown with various TMGa flows by metalorganic chemical vapor deposition to investigate the influence of growth rate on the structural and optical properties. Triple-axis X-ray diffraction measurements show AlInGaN epilayers have good crystalline quality. Photoluminescence (PL) measurements show that the emission intensity of AlInGaN epilayers is twenty times stronger than that of AlGaN epilayer with comparable Al content. V-shaped pits are observed at the surface of AlInGaN epilayers by atomic force microscopy (AFM) and transmission electron microscopy (TEM). High growth rate leads to increased density and size of V-shaped pits, but crystalline quality is not degraded.

PACS: 68.65.+g; 78.55.Cr; 81.15.Gh

Keywords: A1. Triple-axis X-ray diffraction; A1. Atomic force microscopy; A3. Metalorganic chemical vapor deposition; B1. AlInGaN Quaternary alloys

1. Introduction

The group III-nitride wide-band-gap semiconductors have been recognized as leading materials for many optoelectronic devices, such as blue ultraviolet (UV) light-emitting diodes (LEDs), laser diodes (LDs), and high-temperature/high-power electronic devices. Nearly all the high-efficiency blue ultraviolet LEDs and LDs use InGaN quantum wells (QWs) with InGaN or GaN barrier layers. However, AlInGaN quaternary alloy has attracted much research interest because use of this quaternary material should allow almost independent control of the lattice mismatch and band offset in AlInGaN-based heterostructures [1]. Enhanced luminescence in InGaN multile quantum wells with quaternary AlInGaN barriers was demonstrated, in which emission mechanism

*Corresponding author. Tel.: +8610-82304586 ; fax: +8610-82305033.
E-mail address: jpliu@red.semi.ac.cn (J.P. Liu).

0022-0248/$ - see front matter © 2003 Elsevier B.V. All rights reserved.
doi:10.1016/j.jcrysgro.2003.09.007

was considered to change from localized state based to that of a conventional quantum well structure [2–4].

High-power UV LEDs are needed for efficient pumping of phosphors for solid-state white-light devices. UV LEDs with AlGaN QWs as active layer have very low efficiency. However, by introducing In into AlGaN, a similar effect to that obtained in InGaN QWs is expected for quaternary AlInGaN. In fact, enhanced luminescence in quaternary AlInGaN with In-segregation effect have been reported by several authors [5–7].

Although UV LD and LED with AlInGaN-based quantum wells structures have already been demonstrated, fewer reports are available on AlInGaN material properties and optical characteristics. Especially, few authors mentioned the detailed parameters about the crystalline quality of quaternary AlInGaN, such as FWHM of X-ray rocking curve or FWHM of photoluminescence (PL) spectrum. In this paper, AlInGaN quaternary alloys were grown with different TMGa flows. Triple-axis X-ray diffraction (XRD) and PL were used to study the material and optical properties of AlInGaN quaternary epilayers. The surface morphology of AlInGaN quaternary alloy was observed using atomic force microscopy (AFM). Cross-section transmission electron microscopy (TEM) was used to study the pits formation. The effect of growth rate on the structural and optical properties of AlInGaN quaternary alloy was discussed.

2. Experimental procedure

The quaternary AlInGaN epilayers were grown by low pressure metalorganic chemical vapor deposition (MOCVD). A 3 μm GaN template layer was first deposited on the sapphire substrate with a 25 nm low temperature GaN buffer layer, followed by the deposition of a 250 nm AlInGaN epilayers. The growth temperature and pressure for the underlying GaN epilayer were 1040°C and 76 Torr, respectively. Ammonia (NH_3), trimethylaluminum (TMAl), trimethylgallium (TMGa) and trimethylindium (TMIn) were used as precursors. H_2 was used as carrier gas. The molar flows of TMGa during AlInGaN growth were 3, 6, 10, 13 μmol/min for the R1, R2, R3 and R4 samples, respectively. The ratios of TMAl to TMGa and TMIn to TMGa were held constant. Growth rate of sample R1, R2, R3 and R4 is 2.9, 5.4, 8 and 11.8 nm/min, respectively, obtained from the in situ laser reflection spectrum.

Triple axis X-ray diffraction was carried out on a Rigaku SLX-1AL to obtain the composition and to evaluate crystalline quality of AlInGaN epilayers. The 325 nm line of an He–Cd laser was used as an exciting source for the photoluminescence (PL) measurements. A tapping mode AFM (Digital Instruments Nanoscope II) was used to obtain the AFM images. The observed area was $3 \times 3\,\mu m^2$. Cross-section TEM was used to study the pits formation.

3. Results and discussion

Lattice constant can be obtained by triple-axis $2\theta/\omega$ scan, and the FWHM of triple-axis ω scan reflects a degree of crystalline quality [8]. Fig. 1 shows (0 0 0 2) triple-axis $2\theta/\omega$ X-ray diffraction patterns for the four AlInGaN samples with different growth rates. The peaks at 34.56°C originate from the underlying GaN layers and all AlInGaN peaks locate at the left side of the GaN peaks. This indicates the AlInGaN epilayers undergo the compressive strain, which, however,

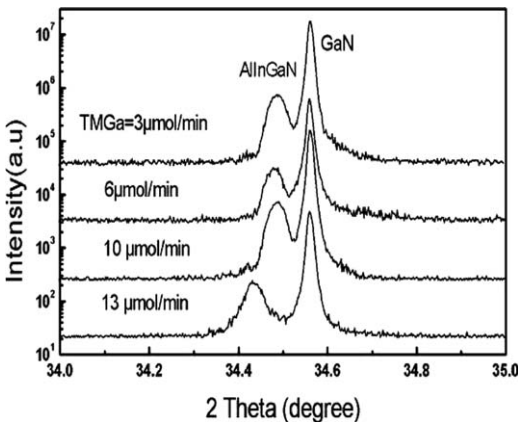

Fig. 1. Triple-axis (0 0 0 2) $2\theta/\omega$ XRD patterns of AlInGaN epilayers grown with various TMGa flows.

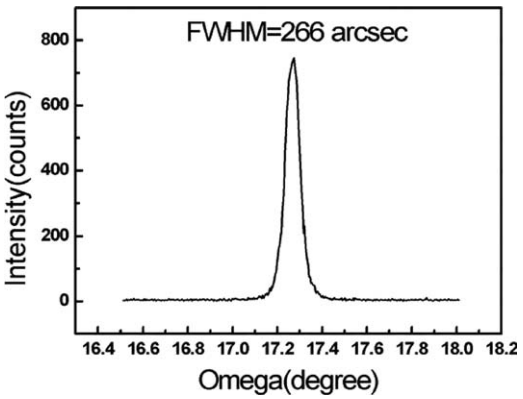

Fig. 2. Triple-axis X-ray ω scan of the AlInGaN peak in sample R1.

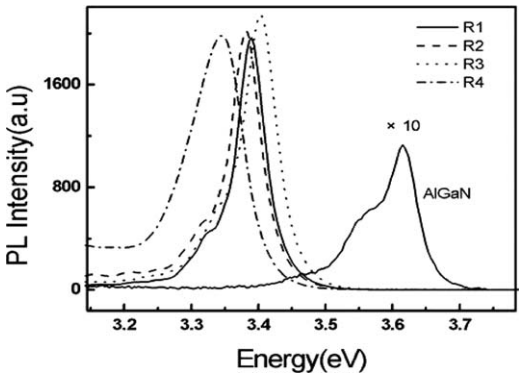

Fig. 3. Room temperature PL spectra for Al0.1Ga0.9N and AlInGaN epilayers grown with various TMGa flows.

is very small. The largest strain experienced by the R4 sample is 3.6×10^{-3}. The other samples have almost equal strain, suggesting the same c-axis lattice constant. Fig. 2 shows triple-axis X-ray ω scan of the AlInGaN peak in sample R1 with a full-width at half maximum (FWHM) of 266 arcsec, indicating good crystalline quality. The FWHM of triple-axis X-ray ω scan of the underlying GaN layer is 280 arcsec. To our knowledge, this narrow FWHM value is the best result obtained from quaternary AlInGaN epilayer up to now. ω scans of other samples have almost the same FWHM, which indicates that crystalline quality is not degraded with increasing growth rate.

Fig. 3 shows room temperature PL spectra for these AlInGaN epilayers. The Al and In contents of sample R1, R2 and R3 are estimated to be 0.075 and 0.04, respectively. Al contents are obtained based on the Rutherford backscattering spectrometry (RBS) measurement for the previously grown samples with the same TMAl, TMGa, and ammonia flows. In contents are obtained based on the measurement of the lattice constant. In addition In contents are confirmed by room temperature PL peak energy. It is assumed that the aluminum and gallium incorporation rate is same at different growth rates. The In content of sample R4 lightly increases to 0.05. This result suggests the In incorporation is not enhanced with the increase of TMGa flow until TMGa flow reaches 13 μmol/min which is the TMGa flow for sample R4. This trend is different from the observation of InGaN growth. This may be due to the effect of Al incorporation because the In–Al–N bond is stronger than In–Ga–N bond. Hirayama et al. [9] also observed much more In was incorporated into AlInGaN epilayers compared with InGaN because of the effect of Al incorporation. All samples show strong band edge emission peaks as we can see in Fig. 3. The emission intensity is twenty times stronger than that of AlGaN epilayer with comparable Al content as shown in Fig. 3. The enhanced emission is due to the In-segregation effect as reported by other authors [5–7]. The peak position for sample R1 is at 3.39 eV and the narrow FWHM of 46.5 meV confirm good crystalline quality. The FWHM of sample R4 increases to 99.4 meV and the integral emission intensity is twice more than that of sample R1 because of larger compositional fluctuations.

Fig. 4 shows AFM images of these AlInGaN epilayers. The surface morphologies of these samples show atomic steps besides hexagonal pits. The pit has a hexahedron cone morphology as shown in a typical SEM image in Fig. 5. The surface region outside V-shaped pits is very smooth, indicating step-flow growth. The density and the size of V-shaped pits in these samples are summarized in Table 1. The density and the size increase with increasing growth rate. Fig. 6 is a

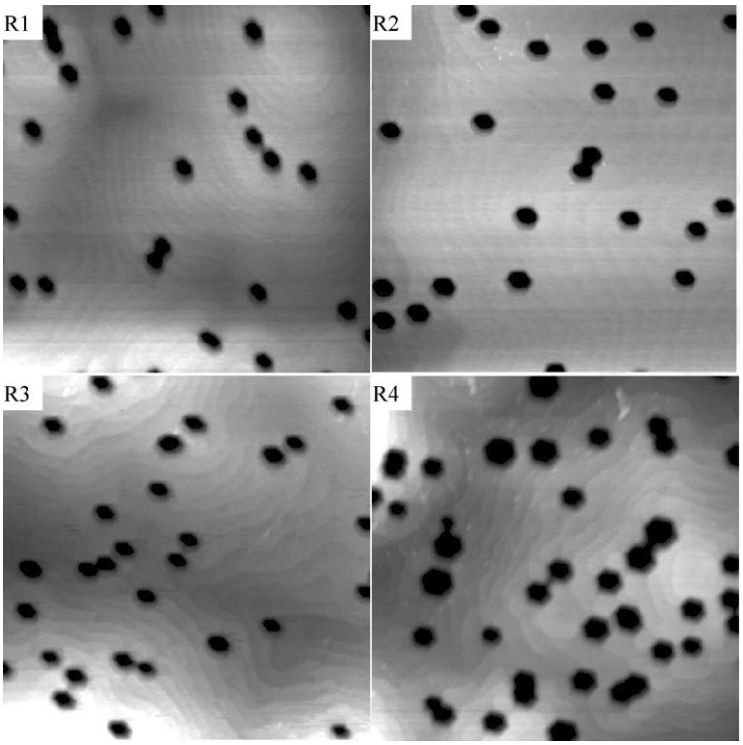

Fig. 4. AFM images of the surface morphologies of AlInGaN epilayers, The scan area is $3 \times 3\,\mu m^2$.

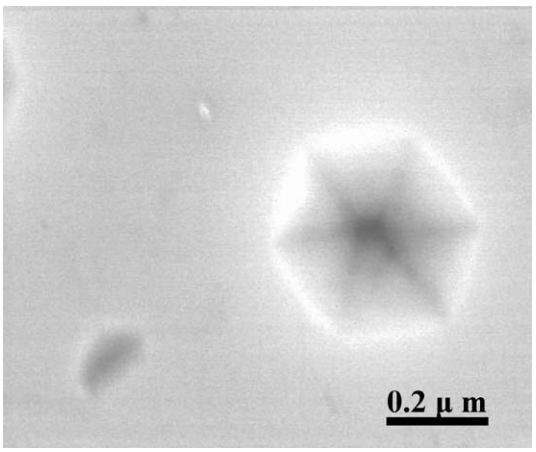

Fig. 5. A typical SEM image of V-shaped pit in AlInGaN epilayer.

typical [10–12] cross-sectional dark-field TEM image of AlInGaN epilayer and underlying GaN template layer. It can be seen that each pit is associated with a threading dislocation from the underlying GaN template layer at its vertex. Pits with similar morphology have been reported previously in InGaN/GaN multiple quantum wells and bulk InGaN film [10–12]. The strain energy induced by the lattice mismatch between InGaN and GaN and the reduction of surface mobility due to the low growth temperature of InGaN are major attributors in the pit formation. We suggest that V-shaped pits in our AlInGaN epilayers have the same formation mechanism due to the similar growth conditions. In atoms tend to congregate in the dislocation core areas due to the low growth temperature. Thus local In segregation may slow down or inhibit the crystal growth in this area, which initiates the pit formation. It has also been proposed that pits start at thread dislocations or In-rich dots in InGaN/GaN multiple quantum wells and bulk InGaN film [10–12]. Surface adatoms have longer time to migrate and thus to find energetically favorable sites before being incorporated into alloy thereby enhancing two-dimensional growth at lower growth rate, which may suppresses the In segregation and also the

Table 1
Summary of AFM results of V-shaped pits in AlInGaN epilayers grown with various TMGa flows

Sample no.	Growth rate (nm/min)	Pit density (cm^{-2})	Pit width (nm)	Pit depth (nm)	RMS (nm) (for $3 \times 3\,\mu m^2$)
R1	2.9	2.3×10^8	234	33	4.4
R2	5.4	2.4×10^8	234	45	5.7
R3	8	3.1×10^8	280	54	8.7
R4	11.8	4.0×10^8	300	115	15.3

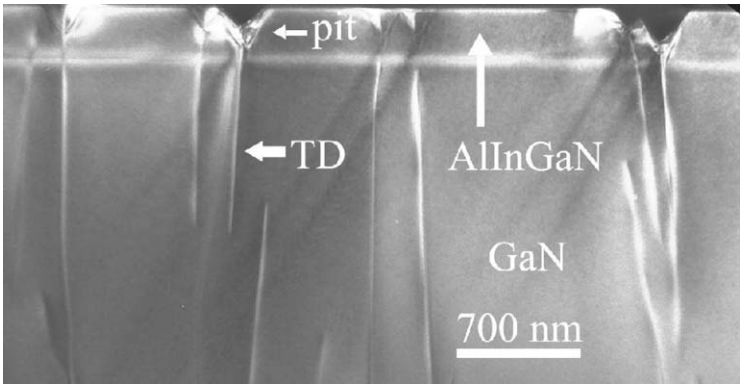

Fig. 6. A typical (10–12) cross-section TEM image of AlInGaN epilayer.

pits formation. On the other hand, pits are more easy and thus more early to form during AlInGaN growth at higher growth rate. That may be the reason why the density and the size of V-shaped pits increase with increasing growth rate. Further investigation about V-shaped pits is underway.

4. Conclusion

AlInGaN quaternary epilayers have been grown with different TMGa flows by MOCVD. Triple-axis X-ray diffraction measurements show AlInGaN epilayers have good crystalline quality, which doesn't degrade with increasing growth rate. Intense UV emission at wavelengths in the range of 360–370 nm has been obtained. The In incorporation doesn't increase with increasing growth rate until TMGa flow reaches 13 μmol/min. The density and the size of V-shaped pits are found to increase with increasing growth rate.

Acknowledgements

The authors gratefully acknowledge Dr. Y.L. Wang for his help in AFM measurement.

References

[1] M. Asif Khan, J.W. Yang, G. Simin, R. Gaska, M.S. Shur, H.-C. zur Loye, G. Tamulaitis, A. Zukauskas, Appl. Phys. Lett. 76 (2000) 1161.
[2] J.P. Zhang, J. Yang, G. Simin, M. Shatalov, M. Asif Khan, M.S. Shur, R. Gaska, Appl. Phys. Lett. 77 (2000) 2668.
[3] A. Chitnis, A. Kumar, M. Shatalov, V. Adivarahan, A. Lunev, J.W. Yang, G. Simin, M. Asif Khan, R. Gaska, M. Shur, Appl. Phys. Lett. 77 (2000) 3800.
[4] M. Shatalov, A. Chitnis, V. Adivarahan, A. Lunev, J. Zhang, J.W. Yang, Q. Fareed, G. Simin, A. Zakheim, M. Asif Khan, R. Gaska, M. Shur, Appl. Phys. Lett. 78 (2000) 817.
[5] H. Hirayama, A. Kinoshita, T. Yamabi, Y. Enomoto, A. Hirata, T. Araki, Y. Nanishi, Y. Aoyagi, Appl. Phys. Lett. 80 (2002) 207.
[6] C.H. Chen, L.Y. Huang, Y.F. Chen, H.X. Jiang, J.Y. Lin, Appl. Phys. Lett. 80 (2002) 1397.

[7] M.-Y. Ryu, C.Q. Chen, E. Kuokstis, J.W. Yang, G. Simin, M. Asif Khan, Appl. Phys. Lett. 80 (2002) 3730.
[8] D. Xu, Y. Wang, H. Yang, L. Zheng, J. Li, L. Duan, R. Wu, Sci. China (a) 42 (1999) 517.
[9] H. Hirayama, A. Kinoshita, A. Hirata, Y. Aoyagi, Phys. Stat. Sol. (a) 188 (2001) 83.
[10] Y. Chen, T. Takeuchi, H. Amano, I. Akasaki, N. Yamada, Y. Kaneko, S.Y. Wang, Appl. Phys. Lett. 72 (1998) 710.
[11] Ig-Hyeon Kim, Hyeong-Soo Park, Yong-Jo Park, Taeil Kim, Appl. Phys. Lett. 73 (1998) 1634.
[12] K. Watanabe, J.R. Yang, S.Y. Huang, K. Inoke, J.T. Hsu, R.C. Tu, T. Yamazaki, N. Nakanishi, M. Shiojiri, Appl. Phys. Lett. 82 (2003) 718.